RSC Advances

ROYAL SOCIETY OF CHEMISTRY

www.rsc.org/advances

Journal Name

RSCPublishing

ARTICLE

Ab Initio Simulation of Pyrene Spectra in Water Matrices

Cite this: DOI: 10.1039/xoxxoooooox

A. Ya. Freidzon,[a] R. R. Valiev[b,c] and A. A. Berezhnoy[d]

Received ooth January 2012,
Accepted ooth January 2012

DOI: 10.1039/xoxxoooooox

www.rsc.org/

The absorption and emission spectra of free pyrene and pyrene in water ice matrix were simulated *ab initio*. Water ice was mimicked by a large cluster of explicit water molecules. The optimum geometries of the ground and excited states, vibrational frequencies, and normal modes were calculated by DFT. The transition energies were calculated by XMCQDPT/CASSCF. *Ab initio* time-dependent Franck–Condon (FC) and time-independent Franck–Condon and Herzberg–Teller (FCHT) approximations were used for the vibronic profiles of the spectra. The absorption spectra of the free molecule and the molecule in the water cluster are well reproduced within the FC approximation. The fluorescence spectrum of the gas-phase pyrene cannot be satisfactorily reproduced within pure FC or within FCHT approximation. However, the fluorescence spectrum of pyrene in the water cluster is satisfactorily reproduced within the FC approximation. Both absorption and emission spectra of pyrene in the water cluster are broadened due to the translations and torques of pyrene in the solvent cage even at low temperatures. This broad but well structured spectrum shape should be taken into account in the identification of PAHs in cometary ice.

Introduction

Polyatomic organic molecules attract the attention of astrochemists as markers of complex prebiotic evolution in the interstellar clouds and celestrial bodies of the Solar system. At the same time, organic molecules can originate from degradation of carbonaceous minerals. For example, polycyclic aromatic hydrocarbons (PAHs) are already detected in carbonaceous chondrites.[1] Among PAHs, pyrene is one of the most interesting species. Although search for pyrene in interstellar molecular clouds gave only negative results,[2, 3] pyrene, however, was tentatively detected in UV spectra of the comet Halley by Clairemidi et al.[4]

Possible existence of luminescence continuum in optical cometary spectra can be explained by the presence of PAH.[5] Observed UV spectra of comets are quite complicated because many organic molecules, molecular ions, and free radicals are luminescent (both in the gas phase and in the ice matrix) in cometary atmospheres. Analysis of observed cometary spectra and assignment of certain spectral features to individual species is an important problem of astrochemistry.

The problem of identification of individual bands can be solved by comparing the observed cometary spectra with the experimental luminescence spectra of hydrocarbons obtained in space-simulated conditions. For example, identification of individual PAH luminescence features is performed by comparison of high-resolution cometary spectra with laboratory PAH spectra obtained in frozen hydrocarbons.[6] Pyrene features were identified based on the tabulated spectrum of pyrene in solid *n*-gexane solution at cryogenic temperatures.[7]

However, it is known that the shape of absorption and, especially, emission spectra of pyrene varies substantially with molecular environment and depends on the excitation method. Thus, excitation with narrow laser lines gives quasi-line emission spectra (fluorescence line narrowing effect[8]), while broadband excitation can give either narrow or broad emission lines depending on the environment, even at cryogenic temperatures.[9, 10] Narrow quasi-line spectra are obtained in Shpolskii matrices (frozen alkanes),[9, 10] while the spectra obtained on pure silica gel or in silica glass matrices exhibit inhomogeneous broadening.[9, 11–13]

The relative intensities of individual emission peaks of pyrene and, therefore, the overall emission bandshape also depend on the environment.[14 –19] This dependence made it possible to use pyrene as an environment polarity probe.[20–28] The difference in the vibronic structure and small, but observable shifts in the excitation energies can be explained by formation of weak intermolecular complexes of pyrene with environment molecules.[26, 29]

It follows that from the above that in order to reliably identify the emitting species in the cometary spectra, one should compare them with the spectra recorded in the matrices mimicking cometary ice rather than in frozen hydrocarbons, under broadband excitation at low temperature and low concentration. If such spectra are unavailable, they can be simulated *ab initio*.

Absorption and emission properties of pyrene. However, pyrene is a challenge for simulations. Pyrene exhibits four UV absorption bands: dark short-axis polarized ^1L_b (~27000 cm^{-1}), bright long-axis polarized ^1L_a (~31000 cm^{-1}), bright short-axis polarized ^1B_b (~37000 cm^{-1}), and very intense long-axis polarized ^1B_a (~43000 cm^{-1}).[30, 31] The B bands can undergo up

to 2000-cm^{-1} shifts depending on the environment, while the shifts of the L bands are no more than 1000 cm^{-1}. As mentioned above, although the absorption and broadband excitation profiles of pyrene in the gas phase,[32, 33] water,[34, 35] solid matrices,[36–39] and organic solutions[7, 35, 40–44] are very similar, its luminescence features (such as relative intensities of the vibronic peaks) in the gas phase,[45–47] aqueous solutions,[35, 48–51] organic solutions,[7, 35, 41–44, 49–51] and solid matrices[9–14,] are quite different.

It is known that the emission spectrum of pyrene does not mirror its absorption profile, which indicates that the emitting electronic state of pyrene differs from the absorbing one. Indeed, the fluorescence polarization studies demonstrate that the emitting state is the short-axis polarized ^1L_b,[31, 40, 43, 27] while the intense absorption occurs to the long-axis polarized ^1L_a. The more remarkable is the fact that the quasiline excitation profile to the emitting state does not mirror the quasiline emission profile, which indicates that pyrene fluorescence is influenced by many nontrivial factors.[52, 53]

In addition to their own emission, PAHs in ice matrices can form photoproducts upon high-energy irradiation,[37, 54–60] and these photoproducts can be even more emissive than parent compounds. However, these reactions are beyond the scope of this paper.

Early simulations of pyrene spectra. Unfortunately, there are only few papers presenting experimental absorption spectra of hydrocarbons and their photolysis products in water ice or solid neon matrices,[37–39] and the emission spectra of pyrene in water ice matrices were not reported yet. One of the possible ways to study the luminescence properties of pyrene is to simulate the absorption and emission band profiles of pyrene molecule with its environment by quantum chemistry mimicking the conditions of cometary atmospheres and nuclei (low concentration, water ice matrix, low temperatures (150–250K), broadband excitation).

The electronic spectra of PAHs are most frequently calculated by TDDFT.[3, 61–63] Thus, in Ref. [3] the conclusions about presence or absence of certain PAHs and their ions in the interstellar clouds were made on the basis of their TD-B3LYP calculated spectra. However, it was shown in Ref. [62] that single-reference methods, such as TDDFT and CIS, predict the dark ^1L_b state of pyrene to lie higher than the bright ^1L_a state, while multireference MCQDPT predicts correct state ordering. The authors of Ref. [64] have tested several methods for the absorption and emission spectra of pyrene. Their research supported the conclusion of Ref. [62] and demonstrated that advanced methods, such as EOM-RI-CC2, CASSCF and CASPT2, MRCI, and MCQDPT give correct state ordering. However, the calculated vertical transition energies were accurate only within 0.2–0.3 eV, which is insufficient for astrophysical applications. Therefore, an accurate and reliable computational technique is required for the electronic absorption and emission spectra of PAHs together with the adequate environment models.

The vibronic profile of pyrene absorption was calculated in Refs. [65–68] based on TDDFT-calculated transition energies within the Franck–Condon and Herzberg–Teller approximations. In Ref. [65], a semiempirical QCFF-PI method was used for the electronic transitions. In Ref. [68], QM/MD method was used to simulate the organic solvent. The vibronic transitions were calculated directly through the Franck–Condon factors. It was shown that both Herzberg–Teller (dependence of transition dipole on the nuclear coordinates) and Duschinsky (normal mode mixing between states) effects only slightly influence the overall absorption profile, at least, at low spectral resolution.

On the other hand, many authors mention that these effects are very important for the dark L_b state.[69–72] In addition, Refs. [27, 43, 53, 73–75] note the importance of nonadiabatic interaction between the S_1 and S_2 excited states of pyrene. The symmetry-forbidden fluorescence from the L_b state can become allowed through certain distortions of the molecule that lift the symmetry restriction. At the same time, this transition can borrow intensity from the nearby allowed S2–S0 transition through nonadiabatic interaction. Both processes result in the appearance of different vibronic peaks. Since both processes are influenced by the environment, this results in the different excitation and emission profiles of pyrene in different matrices.

The goal of this paper is to simulate the absorption and emission spectra of pyrene using accurate high-level *ab initio* methods and to study the effect of water environment on its absorption profile. We try both the time-independent approach with direct summation of Franck–Condon factors for vibronic bandshapes and the alternative time-domain formalism based on Fourier transforms of the Lax's autocorrelation function.[76, 77] We will focus on the accurate simulation of the lowest-energy transitions, mostly on ^1L_a and ^1L_b, because these excited states are responsible for the intense visible fluorescence. In this paper, we will study the influence of Duschinsky and Herzberg–Teller effects on the absorption and emission bandshapes, leaving the nonadiabatic interaction for further investigation.

Computational Procedure

To calculate *ab initio* the vibronic absorption or emission profile within the time-independent formalism in the Franck–Condon approximation, one needs the following data:

1. Fully optimized geometry of the initial state;
2. Fully optimized geometry of the final state;
3. Vibrational frequencies and normal modes in the optimized initial state geometry;
4. Vibrational frequencies and normal modes in the optimized final state geometry;
5. Adiabatic electronic transition energy and transition dipole moment for the desired transition (absorption or emission).

If the Herzberg–Teller effect (dependence of the transition dipole moment on the nuclear coordinates) is to be included in the first order, one also needs the derivative of the transition dipole moment on the nuclear coordinates (a 3N-dimensional vector).

To calculate *ab initio* the vibronic absorption or emission profile within the time-dependent formalism in the linear coupling Franck–Condon approximation, one needs the following data:

1. Fully optimized geometry of the initial state;
2. Vibrational frequencies and normal modes in this geometry;
3. Vertical electronic transition energies and oscillator strengths;
4. The gradients of the final state(s).

The linear coupling approximation used in this work assumes that the hessians of the initial and final states are the same. This is a strong assumption, which works surprisingly frequently (see, for example, Refs. [78–80]). Unfortunately, the time-dependent model used in this paper does not include Herzberg–Teller effect yet.

The equilibrium geometries of the electronic ground state of pyrene (S_0), and its low-lying excited states ^1L_b and ^1L_a in the gas phase were calculated by the density functional theory (DFT) or its time-dependent variant (TD-DFT) using PBE0 functional and 6-311G(d,p) basis set (TD-PBE0/6-311G(d,p)). The same method was used for the vibrational frequencies, normal modes, and gradients. These calculations were performed by GAMESS[81, 82] and FireFly[83] program packages.
The environment effects were simulated by a cluster of explicit water molecules representing the first solvation shell of pyrene. The equilibrium geometries of pyrene in a water cluster were calculated by the same method with 44 explicit water molecules treated quantum-mechanically (Figure 1).

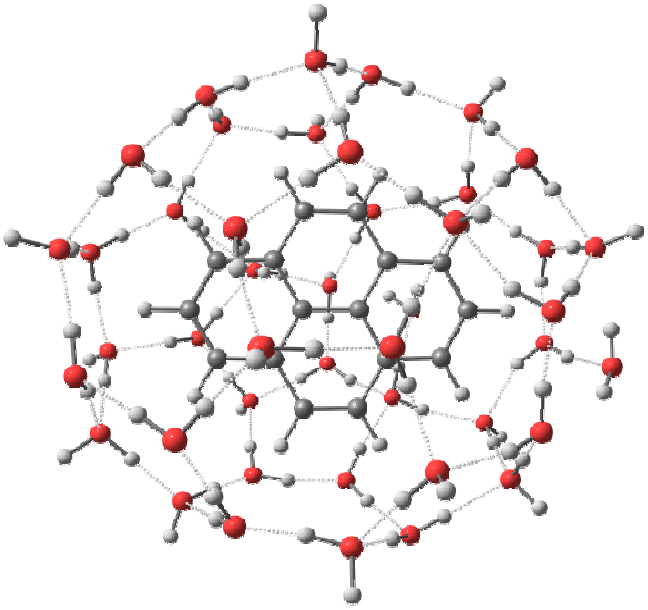

Figure 1. Optimized structure of pyrene in the water cluster.

Such regular clusters are used to obtain reproducible environment effects on the chemical reactivity, electronic and vibrational spectra.[84] The general procedure for generating such clusters is the following. A solute with its nearest environment is cut out of a snapshot of an equilibrated molecular dynamical trajectory. The geometry of the cluster is optimized to a local minimum to ensure that all its vibrational frequencies are real.
It was observed that water forms sort of a cage around hydrophobic compounds. An excellent example of such cage is shown in Fig. 3 of Ref. [85]. The same is true for PAHs in water. Therefore, local geometry optimization only slightly changes the geometry of the nearest environment of the solute. Inhomogeneous effects can be simulated by averaging over statistically significant number of such clusters. However, we consider a single cluster as a representative example in order to demonstrate the effect of water environment on the vibronic bandshapes of pyrene.
The effect of the second and other solvation shells or bulk solvent can be included through polarizable continuum model (PCM). However, this may be important only for the position of the electronic origin. In this work, we focus on the effects of the nearest environment of pyrene in the water ice.
The energies and oscillator strengths for the vertical electronic transition to the five lowest-lying excited states were calculated by state-averaged complete active space self-consistent field with extended multi-configurational quasi-degenerate perturbation theory[86] with the same basis set. Previously, we successfully used this method for excited states,[87–90] and it proved to be very accurate and reliable. The active space consisted of 12 electrons and 10 π orbitals state-averaged over 8 singlet states (XMCQDPT2/SA(8)-CASSCF(12,10)). XMCQDPT2 calculation was performed with an effective Hamiltonian including 30 states. These calculations were performed using FireFly program package.[83]
The vibronic structure of absorption and emission bands of pyrene in the Franck–Condon approximation was calculated through a time-domain formalism of Heller[76] within the double harmonic parallel-mode approximation.[91–93] Similar approach is used by Petrenko and Neese[94] and by the group of Barone.[95, 96] Our calculations were performed using KTS program by the courtesy of Dr. A.V. Scherbinin. We call this procedure Procedure 1.
We constructed the absorption profiles of five excited states of the isolated pyrene molecule and Py·44H_2O cluster using their TDDFT gradients and ground-state DFT Hessians and XMCQDPT2 vertical excitation energies. Next, the area of each absorption band was normalized to its oscillator strength and the bands were added together to give the final spectrum. For the emission spectrum, we used the energy of the 0–0 transition calculated by XMCQDPT, the geometries of the ground and ^1L_b states and Hessian of the ^1L_b state calculated by TDDFT. The emission spectrum was not normalized.
To check the validity of the approximations utilized together with the time-domain formalism, the same spectra of the isolated pyrene molecule were calculated in the Franck–Condon and Herzberg–Teller approximation within the time-independent approach using FCclasses program.[97–102] We call this procedure Procedure 2. Similarly to Procedure 1, the 0–0 transition energies were calculated by XMCQDPT, while the geometries and Hessians were calculated by DFT and TDDFT. Since these calculations require Hessians of each state of interest, we did not go beyond the ^1L_b and ^1L_a states. In this case, Gaussian09 program[103] was used for geometries, Hessians, and transition dipole derivatives. For the emission spectra, the latter were calculated by central differences at the excited-state equilibrium geometries. For the absorption spectra, the transition dipole derivatives were calculated similarly through the numerical calculation of the excited-state Hessian at the ground-state equilibrium geometry.

Results and discussion

Molecular structure.

The calculated geometry of pyrene in its ground and excited states agrees well with the values obtained in Ref.[62] Our data are summarized in Table 1. The geometry changes in the excited states agree with the transition dipole directions: in the ^1L_b state the molecule is stretched along the short axis, while in the ^1L_a state it is stretched along the long axis.
The optimized ground-state structure of Py·44H_2O cluster is shown in Figure 1. Similar structures can be found in molecular-dynamical studies of molecules in bulk water. The atomic coordinates of pyrene and water molecules in S_0, ^1L_b, and ^1L_a states are given in Supporting Information. Our calculations show that the structure of pyrene in the water cluster changes only slightly as compared to the gas phase both in the ground and in the excited electronic states (the difference in the bond lengths is less than 0.01 Å).

Table 1. Calculated bond lengths of pyrene in its ground and excited electronic states (transition dipoles of the two excited states are shown by arrows)

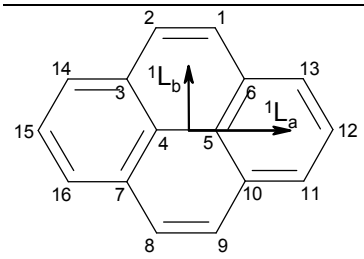

Bond	S_0, Å	^1L_b, Å	^1L_a, Å
1–2	1.35	1.37	1.39
2–3	1.43	1.42	1.40
3–4	1.42	1.44	1.43
4–5	1.42	1.39	1.41
3–14	1.40	1.40	1.42
14–15	1.39	1.40	1.39

Absorption spectra.

The excitation energies for the ^1L_b and ^1L_a states of pyrene calculated by XMCQDPT2 (Table 2) are in excellent agreement with the experimental data. The energy of the ^1B_b state (which appears as S_4 or S_5, depending on the environment) is underestimated by ~0.17 eV. The data of Ref. [64] indicate that this state is better described if diffuse functions are present in the basis set.

Table 2. Calculated excitation (^1L_b, ^1L_a, and ^1B_b states) and emission energies of pyrene in the gas phase and in the water cluster (oscillator strengths in parentheses) compared to the experiment

	Excitation, nm	Exp., nm
Gas phase	367.8 (0.0002)	369 [45], 367 [26]
	317.7 (0.5424)	323 [30, 32, 33, 45]
	275.4 (0.5389)	265 [30, 32, 33, 45]
Py·44H_2O cluster	370.59 (0.0040)	-
	326.03 (0.7976)	332 [34, 35]
	291.43 (0.4375)	274 [34, 35]
	Emission from ^1L_b, nm	Exp., nm
Gas phase	392.8 (0.0006)	372 [45]
Py·44H_2O cluster	396.99 (0.0079)	372 [49, 50]
	Emission from ^1L_a, nm	Exp., nm
Gas phase	343.2 (0.6369)	327 [45]
Py·44H_2O cluster	357.07 (0.7887)	

The excitation energies in the Py·44H_2O cluster are also in good agreement with the experiment, although the error in the position of the ^1B_b state is larger than in the case of isolated pyrene molecule.

On the basis of the calculated transition energies and level positions, we can draw the following scheme of pyrene fluorescence (Figure 2). The molecule is excited to the bright ^1L_a state through Franck–Condon allowed absorption. Next, it relaxes nonadiabatically to the dark ^1L_b state, which, in the equilibrium geometry of the ^1L_a state, lies very close (the energy difference is only 0.4 eV). The molecules further relaxes to the minimum of the ^1L_b state. The emission occurs from the ^1L_b state due to vibrational distortions and dependence of the transition dipole on the nuclear coordinates (Herzberg–Teller effect).

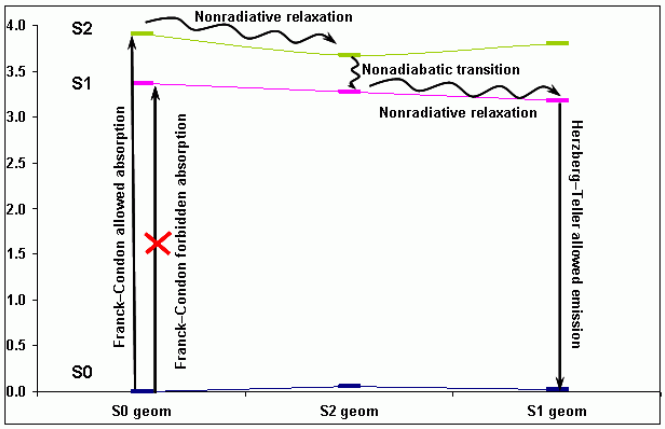

Figure 2. Scheme of pyrene fluorescence.

The vibronic absorption profile calculated by the Procedure 1 for the five lowest-lying states of the gas-phase pyrene is shown in Figure 3b. The agreement of the calculated spectrum with the available experimental spectra of pyrene[32, 33, 36] is very good (the deviation is 1–5 nm).

In order to assess the importance of Herzberg–Teller and Duschinsky effects, we calculated the absorption spectrum in the 25000–35000 cm^{-1} range by the Procedure 2. Simple Franck–Condon calculation with Duschinsky effect showed that the latter is rather small. The spectrum including both Herzberg–Teller and Duschinsky effects is shown in Figure 3c. The overall bandshape is mostly the same, which indicates that Herzberg–Teller effect for the absorption (i.e., for the transition to the bright ^1L_a state) is also small. The entire spectrum, however, is red-shifted by ~1900 cm^{-1} because Procedure 2 uses 0–0 transition energy rather than vertical transition energy used in Procedure 1. To obtain the energy of 0–0 transition in Procedure 2, the adiabatic transition energy is corrected by ΔZPE (~700 cm^{-1}). However, the 0–0 transition energy with ΔZPE correction obtained at the DFT geometries is underestimated by ~1900 cm^{-1}, which explains this red shift.

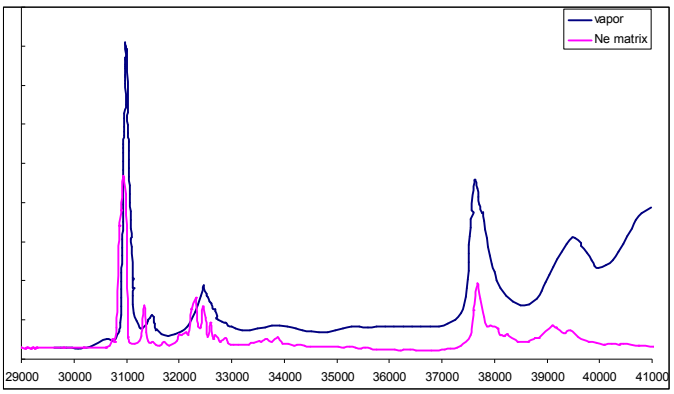

a

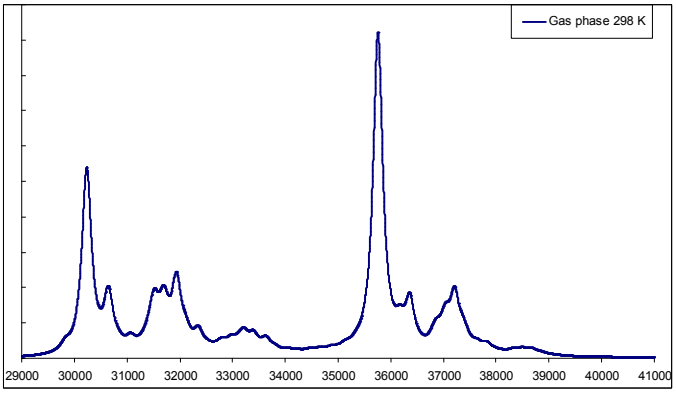

b

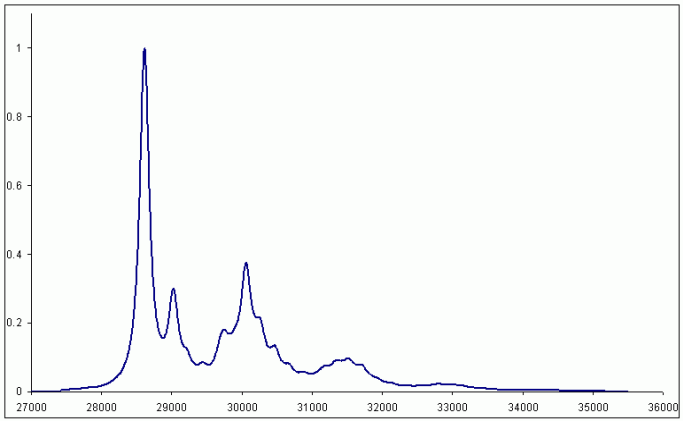

c

Figure 3. (a) Experimental absorption spectrum of pyrene in the gas phase adapted from Ref. [32] and in Ne matrix at 5K adapted from Ref. [36] (b) Calculated absorption spectrum of gas-phase pyrene at 298K (Lorentzian broadening with HWHM ~100 cm^{-1}). (c) Calculated (Procedure 2) absorption to the ^1L_a state taking into account Herzberg–Teller effect (Lorentzian broadening with HWHM ~80 cm^{-1}). Note the origin shift for this spectrum.

Similar results were obtained in Ref. [66] for the three intense absorption bands of pyrene. The authors have found that the overall bandshapes of the bright transitions are well reproduced in the Franck–Condon approximation, and Duschinsky and Herzberg–Teller effects change them only slightly. The same problem with the accuracy of the calculated adiabatic transition energies in this paper is even worse because the authors used TDDFT for this purpose.

Therefore, we can use Procedure 1 for the absorption spectrum of Py·44H_2O cluster, because Procedure 2 is prohibitively expensive and hardly more accurate.

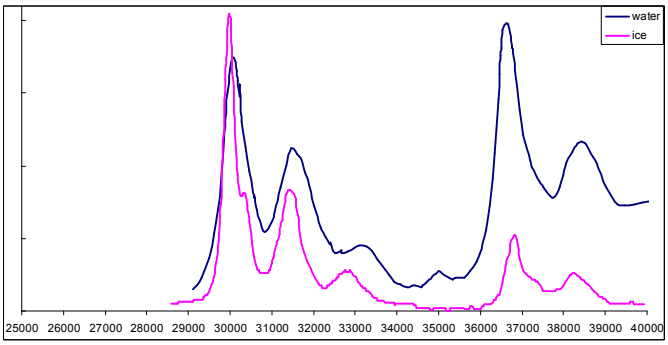

a

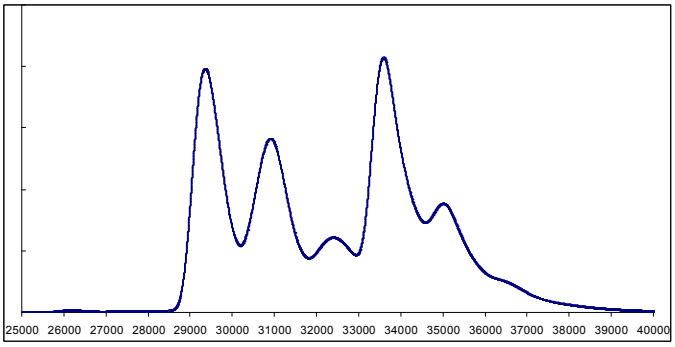

b

Figure 4. (a) Experimental absorption spectrum of pyrene in liquid water at 298K adapted from Ref. [34] and in water ice at 40K adapted from Ref. [60]. (b) Calculated (Procedure 1) absorption spectrum of Py·44H_2O cluster at 4K (Lorentzian broadening with HWHM ~10 cm^{-1}).

The presence of the explicit water cluster (Figure 4b) causes only a slight red shift and a noticeable line broadening. This also agrees with the experimental data.[32–39, 60] In Figure 4b we present the spectrum built for the low temperature (4K) with the Lorentzian broadening parameter of one tenth of that in Figure 3b to demonstrate that the effect is only due to the low-frequency vibrations.

In the Lax's model of vibronic bandshapes, the vibrational modes that have the largest Huang–Rhys factors† contribute to the vibrational progression. The lowest-frequency mode that is responsible for the second (small) peak lying ~400 cm^{-1} above the first one is the mode at 412 cm^{-1} (Figure 5). Other modes responsible for the group of peaks between 31000 and 32000 cm^{-1} are at 1277, 1456, and 1700 cm^{-1}. All these modes belong to the totally symmetric breathing type, A_g.

Similar modes are responsible for the vibronic profile of pyrene in the water cluster. Figures S5, S6, S8 and S9 of Supplementary Material demonstrate that the high-frequency (>100 cm^{-1}) Huang–Rhys factors of pyrene and Py·44H_2O cluster are alike. However, the largest Huang–Rhys factors (~1–18) are observed for the low-frequency modes corresponding to the translations and torques of pyrene in the solvent cage (the mode with the largest Huang–Rhys factor of 18 is shown in Figure S3 of Supplementary Material).

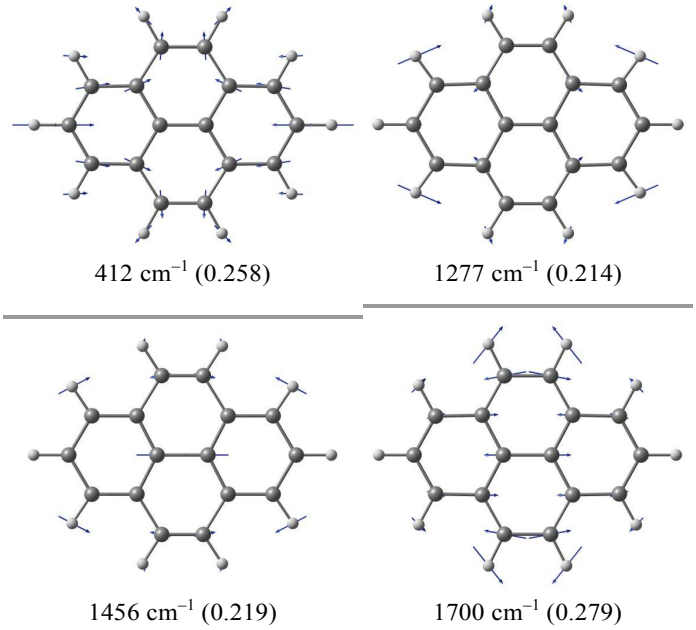

Figure 5. Normal modes of the free pyrene molecule with largest Huang–Rhys factors in the ^1L_a state (in parentheses).

In the Lax's model, the reorganization energy of the transition E_R is expressed via the Huang–Rhys factors S_j and frequencies ω_j as follows: $E_R = \sum_j S_j \hbar\omega_j$. If we compare the contributions to the reorganization energy from individual modes (Figures S6 and S9 of Supplementary Material), we will see that the contributions from the low-frequency modes with large Huang–Rhys factors are comparable to the contributions from the high-frequency modes with Huang–Rhys factors ~0.1–0.2. Therefore, these modes are equally important in spite of two orders of magnitude difference in their Huang–Rhys factors.

In the multimode model, the overall spectrum is a convolution of the vibronic progression originating from each FC active mode (i.e., the modes with nonzero Huang–Rhys factors). If the frequencies of the active modes differ several times, the convolution will result in a progression from the high-frequency mode broadened by the low-frequency vibrations (see, for example, Fig. 5 in Ref. 104). In the case of Py·44H_2O cluster, the progression originates from the FC active breathing modes of pyrene (424, 1294, 1472, and 1712 cm^{-1}) with Huang–Rhys factors ~0.1–0.2, while broadening is due to the librations of pyrene in the water cage and inhomogeneous broadening. Due to this broadening, the progressions from individual high-frequency modes are hidden.

Fluorescence spectra.

The fluorescence spectrum of pyrene has a very peculiar shape depending on the environment polarity. It is now established that this easily observed emission occurs from the dark ^1L_b state, while the emission from ^1L_a can be observed only with special effort.[45] Since the oscillator strength of this transition is almost zero, the emission occurs due to Herzberg–Teller effect. Therefore, only Procedure 2 can be used in this case.

Figure 6 shows the spectra calculated for the absorption from the ground state to the ^1L_b state and for the emission from this state. One can see that each peak in the absorption spectrum has its image in the emission spectrum, although their intensities do not match.

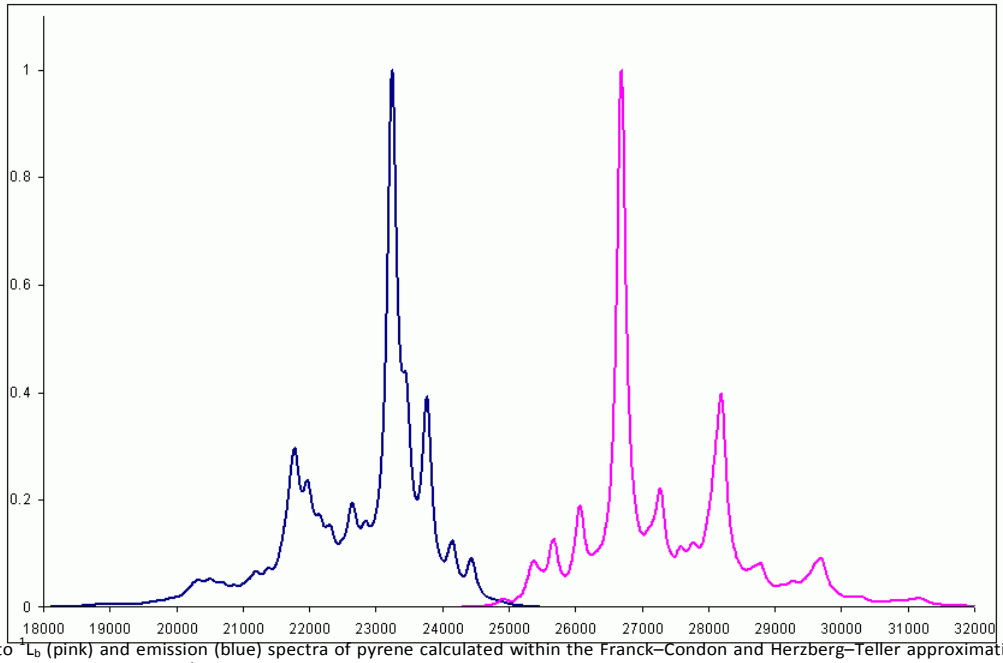

Figure 6. Absorption to ^1L_b (pink) and emission (blue) spectra of pyrene calculated within the Franck–Condon and Herzberg–Teller approximation using Procedure 2 (Lorentzian broadening with HWHM ~80 cm^{-1}).

The calculated 0–0 transition is at 24900 cm^{-1}, its intensity is two orders of magnitude lower than the intensity of visible peaks. Next are several peaks located at 468, 750, 1138, 1444, and 1662 cm^{-1} away from origin. These are so called false origins corresponding to the molecule deformation along the B_{3g} vibrational modes at 462, 750, 1132, 1444, and 1660 cm^{-1} (Figure 7) (frequencies are for the ground state). The largest peak corresponds to the mode at 1660 cm^{-1}. The next peaks are

vibronic progressions from these modes with the totally symmetric vibrations at 815, 1280, and 1459 cm^{-1} (Figure 8).

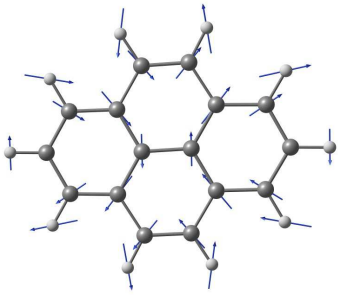

462 cm^{-1}

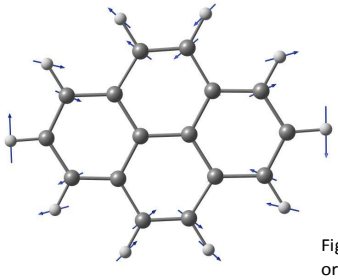

750 cm^{-1}

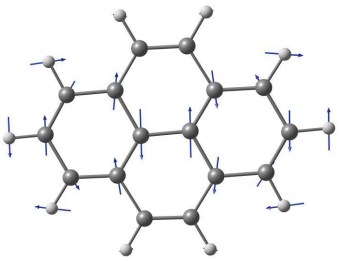

1660 cm^{-1}

Figure 7. Normal modes of the free pyrene molecule responsible for the false origins in the emission spectrum.

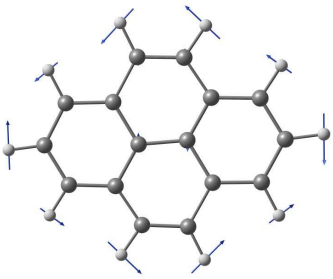

1132 cm^{-1}

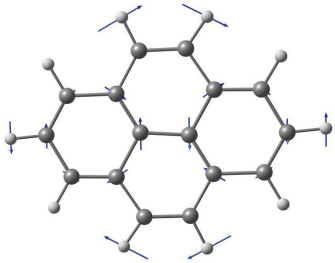

1444 cm^{-1}

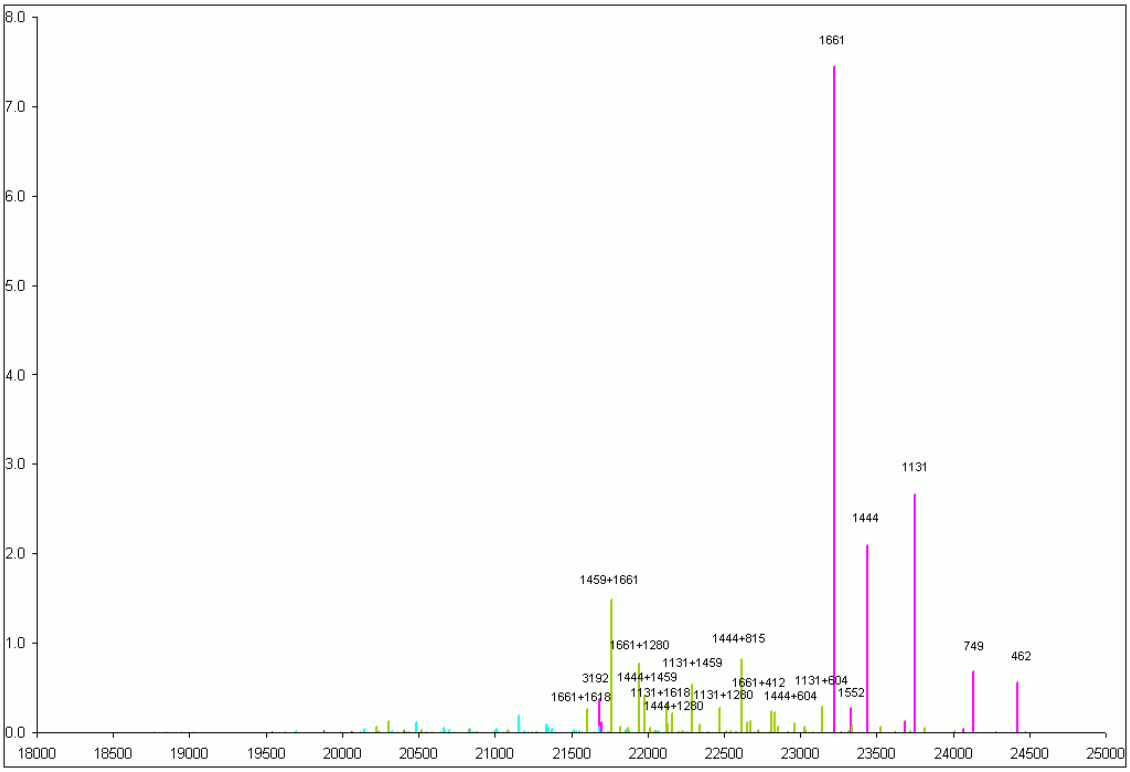

Figure 8. Franck–Condon and Herzberg–Teller intensities of the emission spectrum of pyrene calculated using Procedure 2.

However, the comparison of the calculated spectra with broad-band spectra of pyrene in solutions,[7, 35, 41–44, 49–51] Shpolskii spectra,[9–14, 17, 52, 53] site-selective,[71] or jet-cooled[26] spectra shows that both Franck–Condon and Herzberg–Teller active modes are observed in the experimental spectra with comparable intensities. Therefore, nonadiabatic intensity borrowing that lifts the symmetry restriction for the FC active modes is extremely important in the case of isolated pyrene molecule. This problem was addressed in Refs. [105, 106] with the example of such symmetric molecule as benzene.

It is known that symmetry breakdown in solution or matrix is responsible for the enhancement of weakly allowed electronic

transitions. Obviously, hydrocarbon matrices can form asymmetric environment, especially at low temperatures. Even more so is water, which forms cages around pyrene molecules at low concentrations.

Comparison of the fluorescence spectra in solvents of different polarity indicated that the highest-energy vibronic peak of pyrene in water corresponds to the 0–0 transition. Therefore, the asymmetric environment of pyrene in water results in the enhancement of the 0–0 transition. Indeed, the calculated oscillator strength of the S0→S1 transition of pyrene in the water cluster is more than an order of magnitude higher than that of the free pyrene molecule.

Figure 9 shows the fluorescence spectrum of pyrene in the 44-water cluster calculated by the Procedure 1 and the experimental fluorescence spectra of pyrene in liquid water. The agreement of the spectrum shape is surprisingly good in view of the assumptions underlying Lax's model and Procedure 1. The mode that forms the vibronic progression is 420.3 cm^{-1}, similar to the mode 411.9 cm^{-1} in the isolated pyrene molecule. Its Huang–Rhys factor is 0.315. Two more modes at 817 and 818 cm^{-1} with Huang–Rhys factors of 0.272 and 0.202, respectively, also contribute to the vibronic progression. All these modes correspond to the symmetric long-axis stretch of pyrene molecule, the vibrations that were FC active in the absorption to the ^1L_a state.

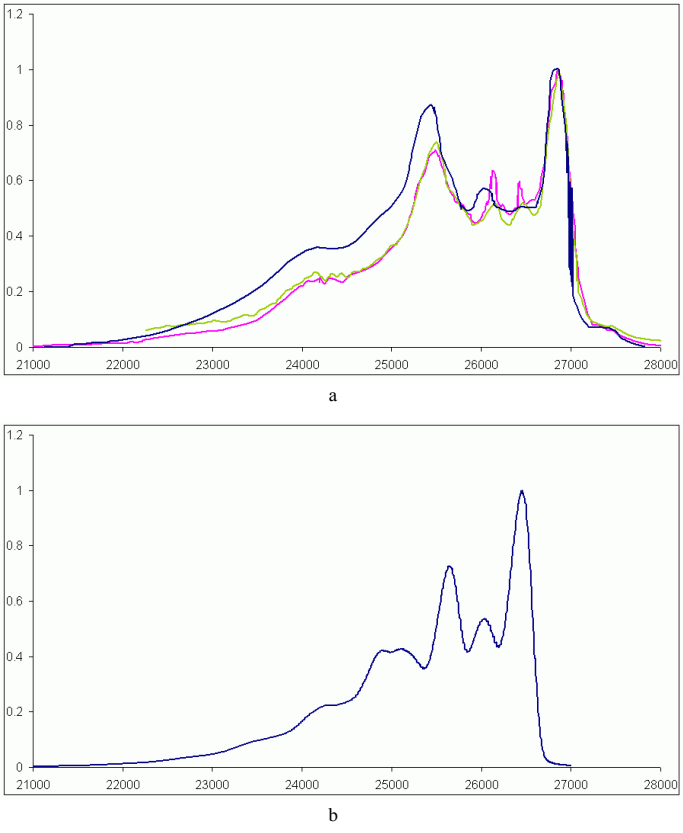

Figure 9. (a) Experimental fluorescence spectra of pyrene in liquid water at 298K adapted from Refs. [35, 48, 49]. (b) Calculated (Procedure 1) fluorescence spectrum of Py·44H_2O cluster at 4K (Lorentzian broadening with HWHM ~10 cm^{-1}).

The calculated spectrum is broad, although it is built at low temperature (4K) and small Lorentzian broadening. Similarly to the absorption spectrum in ice, the broadening is caused by the low-frequency modes with Huang–Rhys factors of 1–6 corresponding to librations of pyrene in the solvent cage. Similar broad bands were observed in such polar matrices as silica gel or inorganic glasses,[9, 11–13] where the effect was attributed to the inhomogeneous broadening.

Temperature dependence of the calculated spectra.

The explicit temperature dependence of the line width of pyrene is not as large as it might be expected. Figure 10 shows the S0→S1 and S0→S2 absorption and S1→S0 emission spectra of pyrene calculated in the HT approximation at 25, 298, and 450K. Similar picture is observed for the S0→S1 and S0→S2 absorption spectra of pyrene calculated in the FC approximation at the same temperatures using Procedure 1 (Figure S2 of Supplementary Material).

As one can see, the temperature broadening is rather small. This can be explained by the fact that the lowest vibrational frequency of pyrene is ~100 cm^{-1}. Therefore, below ~143K, only zero-point levels of all vibrational modes will be populated. At 450K (315 cm^{-1}), the highest frequency mode of pyrene with nonzero populated level is 265 cm^{-1}, and the deformations of pyrene along these modes are very small. All higher-frequency modes are frozen even at 450K and do not contribute to the spectrum broadening.

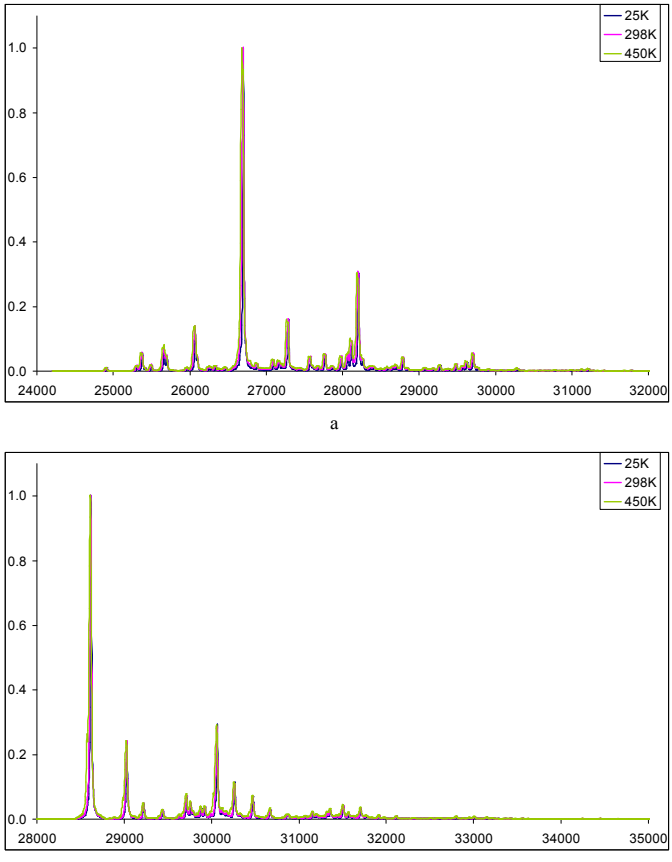

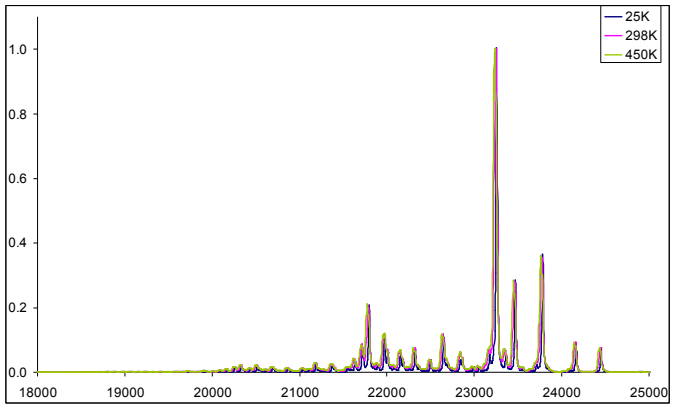

c

Figure 10. Temperature dependence of the Herzberg–Teller spectra of (a) S0→S1, (b) S0→S2, and (c) S1→S0 transitions of pyrene normalized to unit height. Procedure 2, Lorentzian broadening with HWHM ~5 cm^{-1}.

On the other hand, the absorption spectra of Py·44H_2O cluster (Figure 11) depend on temperature substantially, which qualitatively agrees with the experimental data of Ref. [38]. The low-frequency part of vibrational spectrum of Py·44H_2O is very dense; the lowest frequency being ~15 cm^{-1}. This frequency is defreezed at ~20K, and this mode has the largest HR factor of 18. Some other low-frequency modes below 100 cm^{-1} also have nonzero HR factors and, therefore, contribute to the spectrum. The deformations of the entire cluster along these modes are rather large and consist of translations and rotations of pyrene relative to the water cluster.

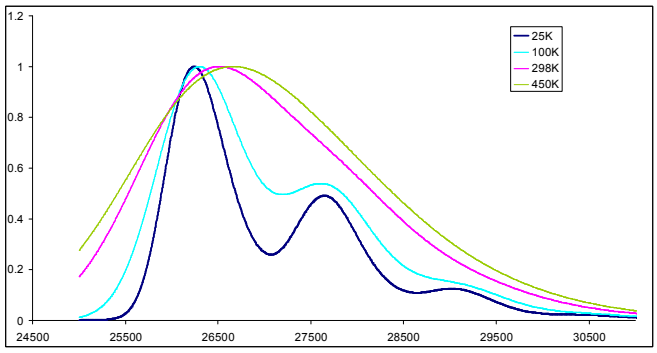

a

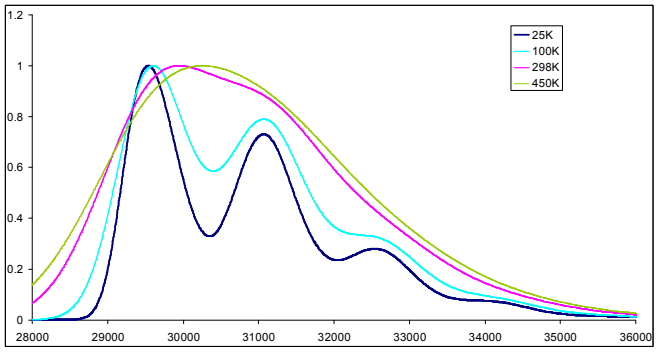

b

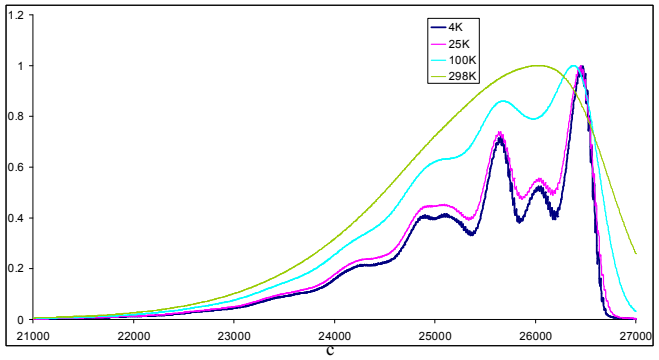

c

Figure 11. Temperature dependence of the Franck–Condon spectra of (a) S0→S1, (b) S0→S2, and (c) S1→S0 transitions of Py·44H_2O cluster normalized to unit height. Procedure 1, Lorentzian broadening with HWHM ~5 cm^{-1}.

Conclusions

The absorption and emission spectra of free pyrene and pyrene in water ice matrix were simulated *ab initio*. The vibronic profile of the absorption spectrum of the free molecule and the molecule in the water cluster are well reproduced within the Franck–Condon approximation. The fluorescence spectrum of the gas-phase pyrene cannot be reproduced within pure Franck–Condon or within Franck–Condon and Herzberg–Teller approximation. Nonadiabatic intensity borrowing from the allowed electronic transition should be included in the model. However, the fluorescence spectrum of pyrene in the water cluster is satisfactorily reproduced within the Franck–Condon approximation. Both absorption and emission spectra of pyrene in the water cluster are broadened due to the translations and torques of pyrene in the solvent cage even at low temperatures. This broad but well structured spectrum shape should be taken into account in the identification of PAHs in cometary ice.

Acknowledgements

This work was supported by the Russian Foundation for Basic Research, project no. 12-03-01103, and by the Presidium of the Russian Academy of Sciences, program no. 22. The calculations were performed using the facilities of the Joint Supercomputer Center of the Russian Academy of Sciences and the Supercomputing Center of Lomonosov Moscow State University. We thank Prof. Dr. H. Linnartz and his co-workers for providing us with the absorption spectra of pyrene in water ice. A. Ya. F. thanks Dr. A. V. Scherbinin (Moscow State University) for the access to the KTS program package and Drs. A. V. Scherbinin and V. G. Avakyan (Photochemistry Center) for valuable discussions.

Notes and references

[a] Photochemistry Center, Russian Academy of Sciences, ul. Novatorov 7a, 119421 Moscow, Russia. E-mail: freidzon.sanya@gmail.com

[b] Department of General and Inorganic Chemistry, National Research Tomsk Polytechnic University, 43a Lenin Avenue, Building 2, 634050 Tomsk, Russia. E-mail: valievrashid@mail.ru
[c] Tomsk State University, 36, Lenin Avenue, 634050 Tomsk, Russia.
[d] Sternberg Astronomical Institute, Lomonosov Moscow State University, Universitetskii prospect 13, 119992 Moscow, Russia. E-mail: ber@sai.msu.ru

† Huang–Rhys factors are dimensionless origin shifts $S_j = \omega_j \Delta Q_j^2/2\hbar$ along the normal mode Q_j, where ω_j is the vibrational frequency and ΔQ_j is the origin shift in normal coordinates. Huang–Rhys factors are also equal to the average number of vibrational quanta created at the frequency ω_j.

Electronic Supplementary Information (ESI) available: Cartesian coordinates (in Å) of S0 state of pyrene in water matrix, figures illustrating the temperature dependence of the calculated absorption and emission spectra, Huang–Rhys factors for pyrene and Py·44H_2O cluster. See DOI: 10.1039/b000000x/

1 O. Botta, J. L. Bada, *Surveys in Geophysics*, 2002, **23**, 411–467.
2 F. Salama, G. A. Galazutdinov, J. Krełowski, L. Biennier, Y. Beletsky, In-Ok Song, *Astrophys. J.*, 2011, **728**, 154.
3 M. Steglich, J. Bouwman, F. Huisken, Th. Henning, *Astrophys. J.*, 2011, **742**, 2.
4 J. Clairemidi, P. Bréchignac, G. Moreels, D. Pautet, *Planet. Space Sci.*, 2004, **52** (8), 761–772.
5 K. I. Churyumov, I. V. Luk'yanyk, V. V. Vlassyuk, N. V. Borisov, *Earth Moon Planets*, 2002, **90** (1), 141–146.
6 I. Simonia, *Astronom. J.*, 2011, **141** (2), 56.
7 L. A. Nakhimovsky, M. Lamotte, J. Joussot-Dubien, *Handbook of Low Temperature Electronic Spectra of Polycyclic Aromatic Hydrocarbons*, Amsterdam: Elsevier, 1989.
8 R. I. Personov, *Sov. Phys. Usp.*, 1975, **18**, 645–646.
9 J. W. Hofstraat, C. Gooijer, N. H. Velthorst, *Appl. Spectrosc.*, 1988, **42** (4), 614–619.
10 J. W. Hofstraat, M. Engelsma, W. P. Cofino, G. Ph. Hoornweg, C. Gooijer, N. H. Velthorst, *Anal. Chim. Acta*, 1984, **159**, 359–363.
11 T. Yamanaka, Y. Takahashi, T. Kitamura, K. Uchida, *Chem. Phys. Lett.*, 1990, **172** (1), 29–32.
12 C. Amine, L. Nakhimovsky, F. Morgan, M. Lamotte, *J. Phys. Chem.*, 1990, **94**, 3931–3937.
13 K. Hara, P. de Mayo, W. R. Ware, A. C. Weedon, G. S. K. Wong, K. C. Wu, *Chem. Phys. Lett.*, 1980, **69** (1), 105–108.
14 L. A. Klimova, *Opt. Spectry*, 1963, **15**, 185.
15 H. Zimmerman, N. Yooρ, *Z. Electrochem*, 1961, **65**, 138.
16 R. N. Nurmukhametov, *Russ. Chem. Rev.*, 1966, **35** (6), 469–486.
17 A. Bree, V. V. B. Vilkos, *Spectrochim. Acta*, 1971, **27A**, pp. 2333–2354.
18 A. Nakajima, *Bull. Chem. Soc. Jpn.*, 1971, **44**, 3272-3277.
19 A. Nakajima, *J. Mol. Spectrosc.*, 1976, **61**, 467–469.
20 S. H. Cuylle, E. D. Tenenbaum, J. Bouwman, H. Linnartz, L. J. Allamandola, *Mon. Not. R. Astron. Soc.*, 2012, **423**, 1825–1830.
21 J. Vanderkooi, J. Callis, B. Chance, *Histochem. J.*, 1974, **6**, 301–310.
22 V. Glushko, M. S. R. Thaler, C. D. Karp, *Archives Biochem. Biophys.*, 1981, **210** (1), 33–42.
23 D. C. Dong, M. A. Winnik, *Photochem. Photobiol.*, 1982, **35**, 17–21.
24 D. C. Dong, M. A. Winnik, *Can. J. Chem.*, 1984, **62**, 2560–2565.
25 K. W. Street, W. E. Acree, *Analyst*, 1986, **111**, 1197–1201.
26 E. A. Mangle, M. R. Topp, *J. Phys. Chem.*, 1986, **90**, 802–807.
27 D. S. Karpovich, G. J. Blanchard, *J. Phys. Chem.*, 1995, **99**, 3951–3958.
28 C. Reichardt, T. Welton, *Solvents and Solvent Effects in Organic Chemistry, Fourth Edition*, Weinheim: WILEY-VCH Verlag GmbH & Co. KGaA, 2011.
29 P. Lianos, S. Georghiou, *Photochem. Photobiol.*, 1979, **30**, 355–362.
30 J. Tanaka, *Bull. Chem. Soc. Jpn.*, 1965, **38**, 86–103.
31 E. W. Thulstrup, J. W. Downing, J. Michl, *Chem. Phys.*, 1977, **23**, 307–319.
32 J. Ferguson, L. W. Reeves, W. G. Schneider, *Can. J. Chem.*, 1957, **35**, 1117–1123.
33 R. S. Becker, I. Sen Singh, E. A. Jackson, *J. Chem. Phys.*, 1963, **38**, 2144–2171.
34 F. P. Schwarz, S. P. Wasik, *Anal. Chem.*, 1976, **48** (3), 524–528.
35 G. B. Ray, I. Chakraborty, S. P. Moulik, *J. Colloid Interface Sci.*, 2006, **294**, 248–254.
36 T. M. Halasinski, F. Salama, L. J. Allamandola, *Astrophys. J.* 2005, **628**, 555–566.
37 J. Bouwman, D. M. Paardekooper, H. M. Cuppen, H. Linnartz, L. J. Allamandola, *Astrophys. J.*, 2009, **700**, 56–62.
38 J. Bouwman, H. M. Cuppen, A. Bakker, L. J. Allamandola, H. Linnartz, *Astron. Astrophys.*, 2010, **511**, A33.
39 J. Bouwman, H. M. Cuppen, M. Steglich, L. J. Allamandola, H. Linnartz, *Astron. Astrophys.*, 2011, **529**, A46.
40 A. Bree, V. V. B. Vilkos, *J. Chem. Phys.*, 1964, **40**, 3125.
41 I. B. Berlman, *Handbook of Fluorescence Spectra of Aromatic Molecules*, Academic Press, N.Y., 1971.
42 J. M. Dixon, M. Taniguchi, J. S. Lindsey, *Photochem. Photobiol.*, 2005, **81**, 212–213.
43 K. Hara. W. R. Ware, *Chem. Phys.*, 1980, **51**, 61–68.
44 H. Du, R.-C. A. Fuh, J. Li, L. A. Corkan, J. S. Lindsey, *Photochem. Photobiol.*, 1998, **68**, 141–142.
45 H. Baba, M. Aoi, *J. Mol. Spectrosc.*, 1973, **46**, 214–222.
46 H. Baba, A. Nakajima, M. Aoi, K. Chihara, *J. Chem. Phys.*, 1971, **55**, 2433.
47 Z. Chi, B. M. Cullum, D. L. Stokes, J. Mobley, G. H. Miller, M. R. Hajaligol, Tuan Vo-Dinh, *Spectrochim. Acta A*, 2001, **57**, 1377–1384.
48 A. Nakajima, *J. Lumin.*, 1977, **15**, 277–282.
49 B. T. Mmereki, D. J. Donaldson, *Phys. Chem. Chem. Phys.*, 2002, **4**, 4186–4191.
50 S. A. Styler, M.-E. Loiseaux, D. J. Donaldson, *Atmos. Chem. Phys.*, 2011, **11**, 1243–1253.
51 K. Kalyanasundaram, J. K. Thomas, *J. Am. Chem. Soc.*, 1977, **99** (7), 2039–2044.
52 K. Cunningham, W. Siebrand, D. F. Williams, C. Orlandi, *Chem. Phys. Lett.*, 1973, **20** (6), 496–500.

53 P. A. Geldof, R. P. H. Rettschnick, G. J. Hoytink. *Chem. Phys. Lett*., 1971, **10** (5), 549–558.
54 S. H. Cuylle, E. D. Tenenbaum, J. Bouwman, H. Linnartz, L. J. Allamandola, *Mon. Not. R. Astron. Soc*., 2012, **423**, 1825–1830.
55 J. Bouwman, A. L. Mattioda, H. Linnartz, L. J. Allamandola, *Astron. Astrophys.*, 2011, **525**, A93.
56 J. Bouwman, H. M. Cuppen, M. Steglich, L. J. Allamandola, H. Linnartz, *Astron. Astrophys.*, 2011, **529**, A46.
57 I. Garkusha, J. Fulara, P. J. Sarre, J. P. Maier, *J. Phys. Chem. A*, 2011, **115** (40), 10972–10978.
58 I. Garkusha, J. Fulara, J. P. Maier, *J. Mol. Struct.*, 2012, **1025**, 147–150.
59 F.-X. Hardy, O. Gause, C. A. Rice, J. P. Maier, *Astrophys. J. Lett.*, 2013, **778** (2), L30.
60 S. H. Cuylle, L. J. Allamandola, H. Linnartz, *Astron. Astrophys.*, 2014, **562**, A22.
61 M. Naganathappa, A. Chaudhari, *Mon. Not. R. Astron. Soc*., 2012, **425**, 490–505.
62 Y. H. Park, B.-S. Cheong, *Current Appl. Phys.*, 2006, **6**, 700–705.
63 R. Ruiterkamp, N. L. J. Cox, M. Spaans, L. Kaper, B. H. Foing, F. Salama, P. Ehrenfreund, *Astron. Astrophys.*, 2005, **432**, 515–529.
64 I. S. K. Kerkines, I. D. Petsalakis, G. Theodorakopoulos, W. Klopper, *J. Chem. Phys*., 2009, **131**, 224315.
65 K. Gustav, M. Storch, *Monatsh. Chem.,* 1992, **123**, 59–62.
66 F. J. Avila Ferrer, V. Barone, C. Cappelli, F. Santoro, *J. Chem. Theory Comput.*, 2013, **9** (8), 3597–3611.
67 M. Dierksen, S. Grimme, *J. Chem. Phys*., 2004, **120**, 3544.
68 M. D'Abramo, M. Aschi, A. Amadei, *J. Chem. Phys*., 2014, **140**, 164104.
69 P. R. Salvi, P. Foggi, E. Castellucci, *Chem. Phys. Lett*., 1983, **98** (3), 206–211.
70 N. Ohta, H. Baba, G. Marconi, *Chem. Phys. Lett*., 1987, **133** (3), 222–229.
71 K. P. Geigle, J. Wolf, G. Hohlneicher, *J. Photochem. Photobiol. A*, 1997, **105**, 183–187.
72 G. Rouille, S. Krasnokutski, F. Huisken, T. Henning, O. Sukhorukov, A. Staicu, *J. Chem. Phys*., 2004, **120**, 6028.
73 Y. Kowaka, N. Nakayama, T. Ishimoto, U. Nagashima, T. Yamanaka, N. Ozawa, M. Baba, *Chem. Phys*., 2012, **400**, 178–184.
74 G. Orlandi, W. Siebrand, *J. Chem. Phys*., 1973, **58**, 4513–4520.
75 S. H. Lin, H. Eyring, *Proc. Natl. Acad. Sci. U.S.A*., 1974, **71**, 3802.
76 E. J. Heller, *Acc. Chem. Res*., 1981, **14**, 368–375.
77 M. Lax, *J. Chem. Phys*., 1952, **20**, 1752–1760.
78 A. V. Bochenkova, L. H. Andersen, *Faraday Discuss*., 2013, **163**, 297.
79 Y. Toker, D. B. Rahbek, B. Klærke, A. V. Bochenkova, L. H. Andersen, *Phys. Rev. Lett*., 2012, **109**, 128101.
80 V. Chashchikhin, E. Rykova, A. Scherbinin, A. Bagaturyants, *Int. J. Quantum Chem*., 2012, **112**, 3110–3118.
81 M. W. Schmidt, K. K. Baldridge, J. A. Boatz, S. T. Elbert, M. S. Gordon, J. H. Jensen, S. Koseki, N. Matsunaga, K. A. Nguyen, S. J. Su, T. L. Windus, M. Dupuis, J. A. Montgomery, *J. Comput. Chem.*, 1993, **14**, 1347–1363.
82 M. S. Gordon, M. W. Schmidt, in *Theory and Applications of Computational Chemistry, the First Forty Years*; Eds C. E. Dykstra, G. Frenking, K. S. Kim, G. E. Scuseria, Amsterdam: Elsevier, 2005, p. 1167.
83 A. A. Granovsky, *Firefly* version 8.0.0, http://classic.chem.msu.su/gran/gamess/index.html.
84 V. Yu. Rudyak, V. G. Avakyan, V. B. Nazarov, M. V. Alfimov, *Nanotechnologies in Russia*, 2009, **4** (1–2), 27–37.
85 N. A. Murugan, Z. Rinkevicius, H. Ågren, *Int. J. Quantum Chem*., 2011, **111**, 1521–1530.
86 A. A. Granovsky, *J. Chem. Phys*., 2011, **134**, 214113.
87 A. Ya. Freidzon, A. V. Scherbinin, A. A. Bagaturyants, M. V. Alfimov, *J. Phys. Chem. A*, 2011, **115** (18), 4565–4573.
88 A. Ya. Freidzon, A. A. Safonov, A. A. Bagatur yants, M. V. Alfimov, *Int. J. Quantum Chem*., 2012, **112**, 3059–3067.
89 R. R. Valiev, E. N. Telminov, T. A. Solodova, E. N. Ponyavina, R. M. Gadirov, G. V. Mayer, T. N. Kopylova, *Chem. Phys. Lett*., 2013, **588**, 184–187.
90 R. R. Valiev, A. N. Sinelnikov, Y. V. Aksenova, R. T. Kuznetsova, M. B. Berezin, A. S. Semeikin, V. N. Cherepanov, *Spectrochim. Acta A: Molecular Biomolecular Spectrosc*., 2014, **117**, 323–329.
91 M. K. Kretov, A. V. Scherbinin, N. F. Stepanov, *Russ. J. Phys. Chem. A*, 2013, **87** (2), 245–251.
92 M. K. Kretov, I. M. Iskandarova, B. V. Potapkin, A. V. Scherbinin, A. M. Srivastava, N. F. Stepanov, *J. Lumin*., 2012, **132**, 2143–2150.
93 P. V. Yurenev, M. K. Kretov, A. V. Scherbinin, N. F. Stepanov, *J. Phys. Chem. A* 2010, **114**, 12804.
94 T. Petrenko, F. Neese, *J. Chem. Phys*., 2007, **127**, 164319.
95 A. Baiardi, J. Bloino, V. Barone, *J. Chem. Theory. Comput*., 2013, **9**, 4097–4115.
96 V. Barone, M. Biczysko, J. Bloino, L. Carta, A. Pedone, *Comput. Theor. Chem*., 2014, **1037**, 35–48.
97 F. Santoro, FCclasses, a Fortran code: available at http://village.pi.iccom.cnr.it/software
98 F. Santoro, A. Lami, R. Improta, V. Barone, *J. Chem. Phys*., 2007, **126**, 184102.
99 F. Santoro, R. Improta, A. Lami, J. Bloino, V. Barone, *J. Chem. Phys*., 2007, **126**, 084509.
100 F. Santoro, A. Lami, R. Improta, J. Bloino, V. Barone, *J. Chem. Phys*., 2008, **128**, 224311.
101 V. Barone, J. Bloino, M. Biczysko, F. Santoro, *J. Chem. Theory Comput*., 2009, **5**, 540–554.
102 J. Bloino, M. Biczysko, F. Santoro, V. Barone, *J. Chem. Theory Comput*., 2010, **6**, 1256–1274.
103 M. J. Frisch, G. W. Trucks, H. B. Schlegel, G. E. Scuseria, M. A. Robb, J. R. Cheeseman, G. Scalmani, V. Barone, B. Mennucci, G. A. Petersson, H. Nakatsuji, M. Caricato, X. Li, H. P. Hratchian, A. F. Izmaylov, J. Bloino, G. Zheng, J. L. Sonnenberg, M. Hada, M. Ehara, K. Toyota, R. Fukuda, J. Hasegawa, M. Ishida, T. Nakajima, Y. Honda, O. Kitao, H. Nakai, T. Vreven, J. A. Montgomery, Jr., J. E. Peralta, F. Ogliaro, M. Bearpark, J. J. Heyd, E. Brothers, K. N. Kudin, V. N. Staroverov, R. Kobayashi, J. Normand, K. Raghavachari, A. Rendell, J. C. Burant, S. S. Iyengar, J. Tomasi, M.

Cossi, N. Rega, J. M. Millam, M. Klene, J. E. Knox, J. B. Cross, V. Bakken, C. Adamo, J. Jaramillo, R. Gomperts, R. E. Stratmann, O. Yazyev, A. J. Austin, R. Cammi, C. Pomelli, J. W. Ochterski, R. L. Martin, K. Morokuma, V. G. Zakrzewski, G. A. Voth, P. Salvador, J. J. Dannenberg, S. Dapprich, A. D. Daniels, O. Farkas, J. B. Foresman, J. V. Ortiz, J. Cioslowski, and D. J. Fox, *Gaussian* 09, Revision A.01, Gaussian, Inc., Wallingford CT, 2009.

104 M. D. Frank-Kamenetskii, A. V. Lukashin, *Sov. Phys. Usp*. 1975, **18**, 391–409.

105 B. F. Minaev, S. Knuts, H. Ågren, O. Vahtras, *Chem. Phys*., 1993, **175**, 245–254.

106 S. Knuts, B. F. Minaev, H. Ågren, O. Vahtras, *Theor. Chim. Acta*, 1994, **87**, 343–371.

